行政院國家科學委員會專題研究計畫　成果報告

可壓縮剪切流之混合層光學性質之數值分析

計畫類別：個別型計畫
計畫編號：NSC94-2212-E-216-008-
執行期間：94 年 08 月 01 日至 95 年 07 月 31 日
執行單位：中華大學機械工程學系

計畫主持人：蔡永培

報告類型：精簡報告

處理方式：本計畫可公開查詢

中　華　民　國 95 年 10 月 26 日

行政院國家科學委員會專題研究計畫成果

可壓縮剪切流之混合層光學性質之數值分析

計畫編號: NCS 94-2212-E-216-008
執行期限: 94/08/01-95/07/31
主持人:蔡永培　中華大學機械與航太工程研究所

Ⅰ.中文摘要

關鍵詞：數值模擬 MacCormack、Godunov 方法; 三度空間剪切混合層 ; 光學

本論文之研究是以數值模擬方法來分析剪切混合層之流場，研究剪切層之物理性質如密度分佈、混合層成長率及渦漩結構現象。數值模擬是交互使用二階準確、顯式之 MacCormack 方法和 Godunov 方法, 來解 3D Navier-Stokes 方程式，比較此剪切混合層的基本特性與實驗數據及其他數值研究者的結果均相符。研究發現共平面光通過成長率是零的剪切層，其光學性質最佳，像差最小。Strehl 比最高。

英文摘要

Keyword：MacCormack Method , Godunov Method , Strehl Ratio

Three-dimensional Navier-Stokes in conserveation law form are solved directly using the second-order, explicit, MacCormack predictorcorrector and Godunov methods alternately for the simulation of spatially developing free and forced shear Layer. The optical effects of coherent structures in the mixing layer are identified. As expected, the far-field optical quality of a laser beam is degraded the most when laser beam passes through the edge of the large eddies. Optical performance can be improved significantly by controlling of the coherent structures in the mixing layer. The shear layer perturbed by periodic forcing with appropriate amplitude is characterized by a region within which the growth rate of the shear layer is zero. It is found that the Strehl ratio ,SR is, the highest in this “non-growth” region of forced situation.

II. Introduction

The plane free shear layer generated by the mixing of co-flowing fluid streams is geometrically simple and is illustrated in Figure1. This simple flow configuration is important in mixing processes and is encountered in many other engineering applications. The extraction of power from high-power gas lasers, for example,

often involves passing the beam through interface between gases of different indices of refraction. Shear layers can produce random phase errors in the beam that can substantially reduce the maximum intensity to which the beam can be focused. Propagation of a laser beam through the atmosphere and aero-optical degradation are two other examples which involve interaction between a mixing layer and a laser beam.The main purpose of this research is to understand the factors which influence optical degradation and to make useful predictions or correlation with respect to the flow parameters. The optical properties of shear layers is a topic of research with applications in high power lasers and optical imaging system. In recent years, it has been shown that large scale structures are intrinsic features in a plane turbulent mixing layer. While there has been some research on the effects of turbulence on laser beams, there has been no study of the

optical effect of large-scale structures as they exist in shear layer development, nor how these effects may be controlled. We are studying the optical effects of large scale structures in forced and unforced situations using periodic motion of a small flap at the trailing edge of the splitter plate.

In order to understand the optical properties of the shear layers, it is necessary to understand their basic fluid mechanics. Many recent experiments have confirmed that large-scale coherent structures are indeed intrinsic features of a plane mixing layer over a wide range of Reynolds numbers [1,2]. The plane mixing layer consists of an array of large eddies of concentrated span wise vorticity. These quasi-two-dimensional large eddies are responsible for the transport of mass and momentum. In the past, the investigation of shear layer optical properties were based on the assumptions of homogeneous turbulence. There has been no study of the optical effects of large-scale structures which exist during the course of shear layer development. One purpose of this work is to identify the optical effects of coherent structures. It is also known from experiments that the shear layer flow pattern can be altered easily by introducing external perturbations near the point of initial mixing [3,4]. Since the spreading rate and the density profile (related to the index of refraction distribution) can be changed drastically by perturbing at a particular frequency with appropriate amplitude, another purpose of this research is to seek out the method of improving optical performance in the far-field by controlling of the mixing layer.

The basic vortex dynamics in a shear layer are essentially inviscid. However, to simulate a free or forced shear layer numerically, 3-D Navier-Stokes equations are solved by alternating the MacCormack explicit, predictor-corrector and Godunov scheme [5,6]. The 3-D Navier-Stokes equations can be solved directly and the density fields obtained are used for shear layer optical property studies.

III. Governing Equation and Numerical Schemes

Based on the assumptions that there are no external heat addition and body forces, the compressible Navier-Stokes equations in 3-D Cartesian coordinates can be written as

$$\frac{\partial \mathrm{U}}{\partial t}+\frac{\partial \mathrm{E}}{\partial x}+\frac{\partial \mathrm{F}}{\partial y}+\frac{\partial \mathrm{G}}{\partial z}=0$$

where U,Q,F and G are vectors given by

$$\mathrm{E}=\begin{bmatrix}\rho\\ \rho u\\ \rho v\\ \rho w\\ E_t\end{bmatrix}$$

$$\mathrm{F}=\begin{bmatrix}\rho u\\ \rho u^2+p-\tau_{xx}\\ \rho uv-\tau_{xz}\\ Puw-\tau_{yz}\\ (E_t+p)v-u\tau_{xy}-v\tau_{yy}-w\tau_{yz}\end{bmatrix}$$

$$\mathrm{G}=\begin{bmatrix}\rho v\\ \rho uv-\tau_{xy}\\ \rho v^2+p-\tau_{yz}\\ \rho vw-\tau_{yz}\\ (E_t+p)v-u\tau_{xy}-v\tau_{yy}-w\tau_{yz}\end{bmatrix}$$

$$H = \begin{bmatrix} \rho w \\ \rho uw - \tau_{xz} \\ \rho vw - \tau_{yz} \\ \rho w^2 + p - \tau_{zz} \\ (E_t + p)v - u\tau_{xz} - v\tau_{yz} - w\tau_{zz} \end{bmatrix}$$

Here x is the streamwise coordinate, y is the cross-stream coordinate and z is in the spanwise direction (see Fig.2). The equations written are in conservation law form represent the conservation of mass, momentum and total energy of fluid motions. The variables $\rho, \rho u, \rho v, \rho w$ and e are mass, streamwise momentum, cross-stream momentum, spanwise momentum and total energy respectively, all per unit volume. P is the pressure. For an ideal gas, the pressure is related to the equation of state $p = (\gamma - 1)\rho\varepsilon$, where ε is the specific internal energy and γ is the ratio of the specific heats, i.e., $\gamma = c_p/c_v$. Throughout this paper the value of γ is taken as 1.40.

The numerical code used in the current work is intended for the direct simulations of the 3-D compressible Navier-Stokes equations with no subgrid scale turbulence model. The code uses finite volume techniques which involves alternating in time the second-order, explicit MacCormack scheme has a lagging phase error and the Godunov scheme has a leading phase error [7], considerable reduction in the phase error can be achieved by temporal switching of these two schemes[8]. The state variables ρ, u , v , w , and e are calculated at the center of each computational cell, which is a cubic mech. A grid system at resolution for $182 \times 32 \times 32$ is adopted, and $\Delta x = \Delta y = \Delta z = 0.02\,\text{cm}$. Note that to calculate the flux terms, second-order extrapolation are made of the primitive variables (ρ, u , v , w , e) from the cell centers to the cell boundaries to give extrapolated values on the two sides of all cell boundaries. On the predictor step, values extrapolated from the left or the bottom or the back side of the cell boundaries are used; on the corrector step, values extrapolated from the right or the top or the front side of the cell boundaries are used. To achieve numerical stability, a simple limiting technique is applied, that is, all extrapolated values of the primitive variables at the cell boundaries must lie between the cell center values at the two adjacent cell centers. If any extrapolated value of a primitive variables does not satisfy this condition, it is replaced by the cell center value which is more closer to it [9].

Two low speed air streams are modeled, each with different enthalpy, so that the density ration is 1.1 at a velocity ratio of 0.5. The two free stream velocities are $U_1 = 7.04 \times 10^3$ cm/sec (M=0.2) and $U_2 = 3.52 \times 10^3$ cm/sec; the densities are $\rho_1 = 1.2019 \times 10^{-3}$ g/cm3, and $\rho_2 = 1.1\rho_1$. A hyperbolic-tangent velocity profile is adopted for the initial streamwise velocity distribution at the splitter plate such that the initial momentum thickness of the shear layer is 0.02cm. However, in the initial density profile there is a discontinuity at the contact surface. The pressure everywhere is 1 atm, the y-component, and the z component of the velocity are zero initially.

Both mass flux and energy flux are kept constant as the inflow boundary conditions. Based on the hypothesis that the top, bottom, back and front boundaries are streamlines, the numerical boundary conditions used there are $v = 0, w = 0, \frac{\partial q}{\partial y} = 0$ and $\frac{\partial q}{\partial z} = 0$, where q is ρ, or u , or e. For the outflow boundary condition, the pressure is assumed to be constant.

It has been shown that in order to resolve the large-scale structures in a mixing layer, unsteady boundary conditions must be applied [10]. In this case, at the inlet plane, a periodic forcing is introduced to simulate the “natural” mixing layer. The forcing frequencies consist of the fundamental frequency and the first three subharmonics of the shear layer. The fundamental frequency satisfies the Strothal number criterion which is derived from Rayleigh’s inviscid, linear stability theory [11]. In this case, the fundamental frequency is 4.227KHZ. Furthermore, the forcing is modified by incorporating random phases to the Rayleigh modes to simulate random pairing of two neighboring vortices [12].

To advance the code in one time step Δt, the numerical stability condition must be applied [5,6]. During this time interval, Δt, waves from neighboring Riemann problems will not interact with each other. In our calculations, $\Delta x, \Delta y$, and Δz are of the order of millimeter, Δt is therefore of the order of microsecond to satisfy the stability condition. Generally, the statistical stationary fluid dynamical results can be obtained after 10,000 time steps. To calculate the time averaged fluid dynamical variables, a time interval of 5,000 time steps is needed.

Ⅳ. Results and Discussions

Figure 3 shows the instantaneous isodensity plot of a 3D free shear layer at velocity ratio 0.5 and density ratio 1.1. Examining this figure carefully, the adjacent structures are connected by braids which are regions of low vorticity and highly strained. The center of the shear layer moves towards the low-speed side. There are more fluid particles entrained from the high-speed side than that from the low-speed side in the mixing region. Entrainment asymmetry is an important feature of the spatial shear layer and this result is consistent with the experimental evidence [13, 14] and other numerical simulations [15]. Figure 4 shows a sequence of instantaneous flow visualization of the density field for the natural shear layer. These figures clearly show the pairing phenomenon between two vortices. This vortex amalgamation process occurs randomly in space and time and it is responsible for the linear growth rate of shear layer. In the fully developed region, statistics of the fluid dynamical variables such as streamwise velocity, rms u-fluctuations, v-fluctuations, and w-fluctuations as well as the Reynolds stress distribution show that the flow is self-similar which are not shown due to limited space. Figure 5 and Figure 6 are plots of isodensity field for the shear layer under fundamental frequency and first subharmonic frequency perturation respectively. Forcing with fundamental or subharmonic frequency produces controlled coherent structures where the growth rate of the forced shear layer is zero. In the non-growing region of the shear layer, amalgamation of neighboring vortices are inhibited and the mixing layer consists of an array of large eddies in the lateral direction with no interactions.. The trends of all fluid dymical results obtained are consistent with experimental and numerical results of others [16, 17] lend full confidence that the code has been validated satisfactorily. The density field then can be used for shear layer optical property studies.

The phase distortation of a coherent light beam plays a very important role in determing the far-field properties of the beam. Coherent structures of the shear layer generate phase

errors in the laser beam passing through it. Basically, the far-field intensity profile is the modulus square of the Fourier transform of the aperture function [18]. The optical effects of the shear layer are calculated by passing a laser beam through it with circular aperture and uniform phase. The far-field focal plane intensity distributions measure the optical quality of the shear layer. The Strehl ratio, SR, which is defined as the ratio of the maximum light intensity of the diffraction pattern to that of the same optical system without aberrations, will be used to evaluate the optical quality quantitatively [19, 20, 21, 22]. Figure 7 gives a typical example plot of the instantaneous Strehl ratio for the natural shear layer. The beam size is larger than that of the flow structure, wide angle scattering due to these fluid fluctuations removes optical energy from the beam and spreads the intensity profile in the far-field. The Strehl ratio is 0.585, more than 40% of peak energy is removed. However if laser beam passing through the non-growing region of the forced shear layer where the large eddies are equal in size, results in the amplitude of the phase variation being small, which in turn improves the optical performance in the far-field. Figure 8 demonstrates this effect. When laser beam passing rough the non-growth region of the shear layer, the lobes in the far-field pattern disappear which is due to partial compensation for the phase errors in this region. The Strehl ratio is 0.921, a significant recovery of SR value.

Ⅴ. Conclusions

1. The simplest and most natural way of modifying the mixing layer is to perturb the layer by external, periodic disturbances.
2. If beam performance improvement is needed in the region near the point of mixing, the method of fundamental frequency forcing should be applied; otherwise the method of subharmonic forcing may be used.

For a forced shear layer in the region of zero growth rate, the optical performance of the shear layer in the far-field is improved significantly. But the thickness of the shear layer in this region is not a important factor controlling the optical quality of the shear layer.

References

1. Brown. G. L., and Roshko, A., “On Density Effects and Large Structures in Turbulent Mixing Layers.” J. Fluid Mech., Vol. 64. 1974, pp. 775－816.
2. Winant,C. D., and Browand, F.K., “Vortex Pairing, Mechanism of Turbulent Mixing Layer Growth at Moderate Reynolds Number,” J. Fluid Mech., Vol. 63. 1974, pp. 237－255.
3. Ho, C. M., and Huang, L.S., “Subharmonics and Vortex Merging in Mixing Layers,” J. Fluid Mech., Vol. 119. 1982, pp. 443－473.
4. Oster, D., and Wygnanski, I., “The Forced Mixing Layer between Parallel Streams,” J. Fluid Mech., Vol. 123. 1982, pp. 91－130.
5. MacCormack, R. W., “The Effect of Viscosity in Hypervelocity Impact Cratering,” AIAA Paper 69－354, 1969.
6. Holt, M., “Numerical Methods in Fluid Dynamics,” Springer-Verlag, Berlin, 1977, pp.29－37.
7. Steger, J. E., and Warming, R. F., “Flux Splitting of the Inviscid Gasdynamic Equations with Application to Finite Difference Method,” J. of Comput. Phys., Vol. 40, 1981, pp.263－

293.

8. Fromm, J. E., “A Numerical Study of Buoyancy Driven Flow in Room Enclosures,” Lecture Note in Physics, Springer-Verlag, Vol. 8, 1971, pp. 120－126.
9. Bogdanoff, D. W., and Brackett, D. C., “A Computational Fluid Dynamics Code for the Investigation of Ramjet-In-Tube Conncepts,” AIAA Paper 87－1978, 1987.
10. Chien, K. Y., Ferguson, R. E., Collins,J. P., Glaz, H. M., and Kuhl, A. L., “A Study of Mixing in Forced Shear Layers with an Euler Code,” AIAA Paper 87-1318,1987.
11. Ho, C. M., and Huerre, P., “Perturbed Free Shear Layers,” Ann. Rev. Fluid Mech., Vol. 16, 1984, pp. 365-424.
12. Sandham, N. D., and Reynolds, W. C., “Some Inlet Plane Effects on the Numerically Simulated Spatially Developing Two Dimensional Mixing Layer,” Turbulent Shear Flows, 1987, pp. 22-4-1－22-4-6.
13. Papamoschou, D., and Roshko, A., “Observations of Supersonic Free Shear Layers,” AIAA Paper 86－0162, 1986.
14. Koochesfahani, M. M., Dimotakis, P. E., and Broadwell, J. E., “Chemically Reacting Shear Layer,” AIAA Paper 83－045, 1983.
15. Grinstein, F. F., Oran, E. S., and Boris, J. P., “Numerical Simulations of Asymmetric Mixing Layer in Planar Shear Flows.” J. Fluid Mech., Vol. 165. 1986, pp. 201－220.
16. Tennekes, H., and Lumley, J. L., “A First Course in Turbulence,” The MIT Press, Massachusetts, 1972, pp.214－215.
17. Riley, J. J., Metcalfe, R. W., “Direct Numerical Simulation of a Perturbed, Turbulent Mixing Layer,” AIAA Paper 80－0274, 1980.
18. Goodman, J. W., “Introduction to Fourier optics,” 1st ed., McGraw－Hill, New York, 1968, p. 395.
19. Born, M., and Wolf, E., “Principles of Optics,” 6th ed., Pergamon Press, New York, 1980, p. 395.
20. Liepman, H. W., and Roshko, A. “Elements of Gasdynamics,” 1st ed., Wiley, New York, 1957, p. 154.
21. Hugo RJ, Jumper EJ. Applicability of the acro-optic linking equation to a highly-coherent, transitional shear layer. Appl Opt 2000;39.
22. Cicchiello JM, Jumper EJ. Low-order representation of fluid-optic interactions associated with a shear layer. AIAA Paper 2001-0952, January 2001.

Fig.1 Example of free shear layer.

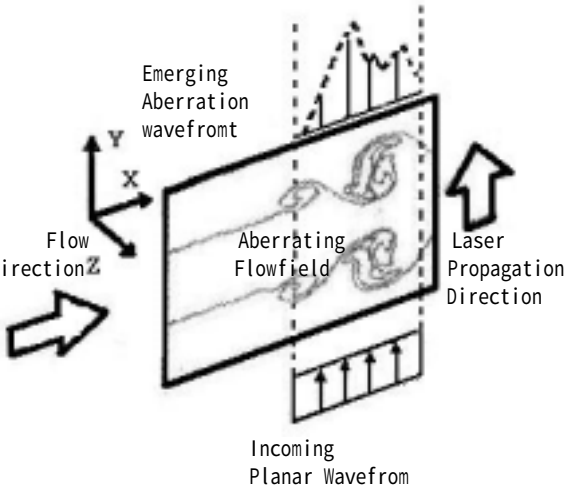

Fig.2 Schematic of a planar wave front propagating through a shear layer.

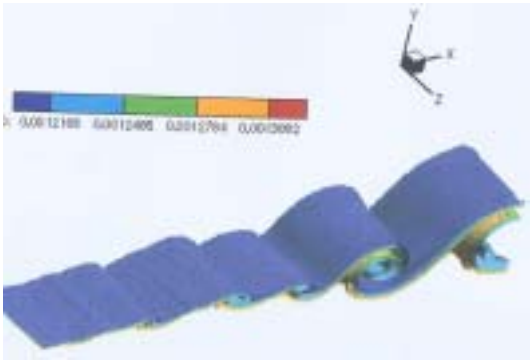

Fig.3 Isodensity plot of a 3D free shear layer at velocity ratio 0.5 and density ratio 1.1.

Fig.6 Isodensity plot for a forced shear layer by first subharmonic frequency.

SR=0.585 λ = 6328A
D = 5.12 cm

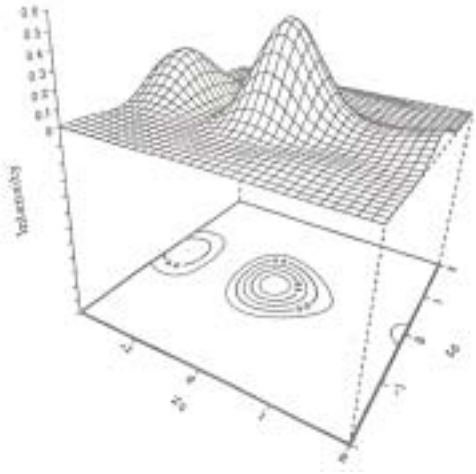

Fig.7 Far field intensity contour with aberrations.

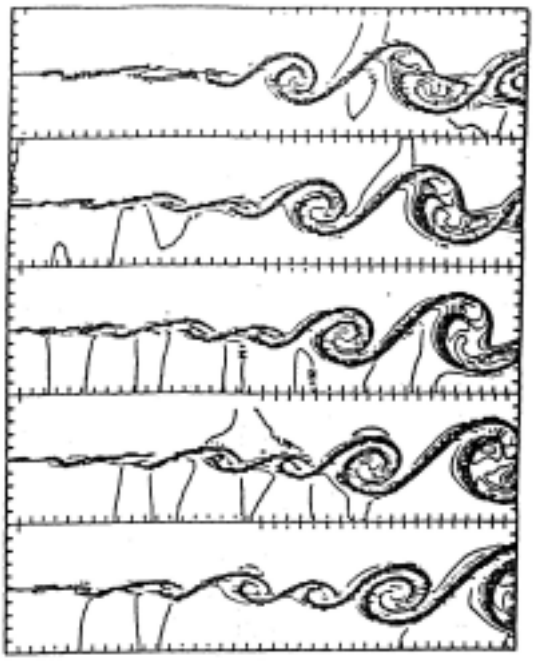

Fig.4 Instantaneous isodensity plot of a shear layer at z=0.

SR=0.585 λ = 6328A
D = 5.12 cm

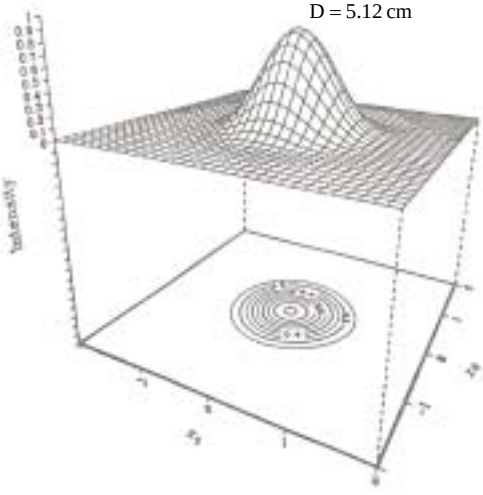

Fig.8 Far field intensity contour produced by the forced shear layer.

Fig.5 Isodensity plot for a forced shear layer by fundamental frequency.